Biophysical Journal Volume 97 August 2009 1225–1231 

# Tracking Molecular Interactions in Membranes by Simultaneous ATR-FTIR-AFM

Jocelyne E. Verity,[†] Neetu Chhabra,[‡] Koneswaran Sinnathamby,[†] and Christopher M. Yip[‡*]
[†]Institute of Biomaterials and Biomedical Engineering and [‡]Department of Chemical Engineering and Applied Chemistry,Terrence Donnelly Centre for Cellular and Biomolecular Research, University of Toronto, Toronto, Canada

ABSTRACT In situ atomic force microscopy (AFM) is an exceedingly powerful and useful technique for characterizing the structure and assembly of proteins in real-time, in situ, and especially at model membrane interfaces, such as supported planar lipid bilayers. There remains, however, a fundamental challenge with AFM-based imaging. Conclusions are inferred based on morphological or topographical features. It is conventionally very difficult to use AFM to confirm specific molecular conformation, especially in the case of protein-membrane interactions. In this case, a protein may undergo subtle conformational changes upon insertion in the membrane that may be critical to its function. AFM lacks the ability to directly measure such conformational changes and can, arguably, only resolve features that are topographically distinct. To address these issues, we have developed a platform that integrates in situ AFM with attenuated total reflection-Fourier transform infrared (ATR-FTIR) spectroscopy. This combination of tools provides a unique means of tracking, simultaneously, conformational changes, not resolvable by in situ AFM, with topographical details that are not readily identified by conventional spectroscopy. Preliminary studies of thermal transitions in supported lipid bilayers and direct evidence of lipid-induced conformational changes in adsorbed proteins illustrates the potential of this coupled in situ functional imaging strategy.

## INTRODUCTION

Recent advances in high-resolution correlated imaging tools have provided tremendous new insights into the mechanisms and function of proteins and biomolecules. Such in situ functional imaging tools are providing researchers with the unique opportunity of performing correlated characterization of protein interactions, often in real-time, and under physiologically relevant conditions, on molecular length scales. This includes direct imaging of protein structure and assembly, in situ measurement of protein association forces, and direct determination of the kinetics of complex formation. We recently demonstrated the potential of coupled confocal-total internal reflection fluorescence-atomic force microscopy (AFM) for examining peptide membrane interactions and membrane dynamics (1–7). However, we, and others have seen that the addition of an extrinsic fluorophore can affect the distribution and dynamics of the parent molecule (3). Moreover, this approach cannot readily provide direct insight into molecular conformation or, in the case of peptide-membrane interactions, evidence of lipid-induced secondary structure changes and/or alterations to lipid structure or packing. For example, although we previously reported direct evidence of membrane-induced fibrillogenesis of the A$\beta$ peptide, we could only infer that these fibrils were $\beta$-structured (8).

A technique that is particularly useful for examining peptide-membrane interactions, lipid dynamics, and membrane protein conformation is attenuated total reflection infrared (ATR-IR) spectroscopy (9,10). Recent work includes studies of adrenocorticotropin (11,12), bomebesin (13), calcitonin (14), antibiotic peptides such as the gramicidins (15–17), amphiphilic peptides such as melittin (18), fusion peptides including gp41 of human immunodeficiency virus (19,20), and segments of transmembrane proteins such as phospholamban (21).

This prompted us to design a platform that combines the three-dimensional topographical imaging capabilities of AFM with infrared spectroscopy using a multibounce germanium (Ge) internal reflection element (IRE) to examine protein-membrane interactions. Recently, a similar configuration based on a single-bounce hemispherical ZnS IRE was used to examine inorganic crystal growth and dissolution dynamics (22).

To validate the ability of this platform to perform simultaneous topographical and spectroscopic analysis, we examined the thermal phase transition behavior of multilamellar DPPC lipid bilayers. Upon heating, AFM imaging revealed topographical details consistent with the gel-fluid phase transition, which reversed upon cooling. Concomitant shifts in the peak positions of the $\nu_{as}(CH_2)$ and $\nu_s(CH_2)$ modes confirmed changes to the local order of the lipid tails upon heating and cooling. We then examined the interaction between the soluble protein, $\beta$-lactoglobulin ($\beta$LG), and various model membranes to examine how protein conformation may be changed upon membrane association. Although the AFM data were unremarkable in that no topographical features were resolved that could be attributed to $\beta$LG association or deposition, the ATR-IR spectra confirmed that the protein had in fact inserted into the membrane while Fourier self-deconvolution (FSD) analysis provided direct evidence of lipid-dependent $\beta$LG folding.

*Submitted February 20, 2009, and accepted for publication June 11, 2009.*

*Correspondence: christopher.yip@utoronto.ca

Editor: Peter Hinterdorfer.



0006-3495/09/08/1225/7 $2.00

doi: 10.1016/j.bpj.2009.06.013

These experiments demonstrate the power of a correlated AFM and ATR-Fourier transform infrared spectroscopy (FTIR) platform and portend its application to study peptide-membrane interactions, including membrane-induced aggregation and antimicrobial peptide insertion and folding.

## METHODS AND MATERIALS

### Integrated setup

Our combined system integrated a retrofitted large-area dual-range vertical engage AFM "J" scanner (116 $\mu$m $\times$ 116 $\mu$m maximum lateral scan area) (Dimension scanner; Digital Instruments/Veeco, Santa Barbara, CA) into the sample compartment of an infrared spectrometer (Magna 750 spectrometer; Nicolet/Thermo Electron, Madison, WI) equipped with a DTGS detector, a mid-range IR source, and KBr beamsplitter (see Fig. 1). Due to spatial constraints within the sample compartment of the spectrometer, the existing backplane that holds the AFM scanner was replaced by a custom-built dovetail equipped with a stepper motor. Coarse vertical positioning of the scan head over the sample was performed by driving the stepper motor with a motion controller (Newport ESP 300; Newport, Irvine, CA) while simultaneously monitoring the low-voltage $Z$ signal (using a Signal Access Module; Digital Instruments/Veeco, Santa Barbara, CA) from the scanner through a customized Labview program (version 7.1, National Instruments, Austin, TX). This particular signal reflected either the tip deflection or amplitude damping, depending on the operating mode (contact/intermittent contact) of the AFM. In this way, we could monitor tip approach to the sample. Once contact with the sample was made, as determined by a predetermined tip deflection or amplitude damping, the commercial AFM software would engage and control sample scanning. To accommodate the AFM scanner, dovetail assembly, and stepper motor within the FT-IR sample chamber, the original chamber cover was replaced by a custom-built enclosure that allowed the compartment to be continually purged with dry air from a Balston 7545-FTIR Purge Gas Generator (Thermo-Fisher Scientific, Markham, Ontario, Canada).

A 50 $\times$ 20 $\times$ 2 mm rectangular Ge IRE with a 45° cut surface (Sigma-Aldrich Canada, Oakville, Ontario, Canada) was used for this study. Advantages of a Ge IRE include its relative high hardness compared to other materials, a smaller depth of penetration (0.2–1 $\mu$m) due to its high index of refraction ($n = 4$), and a 23° critical angle. Ge IREs have been used extensively in ATR-IR studies of peptide-membrane interactions (9). The IRE was fitted to a custom-fabricated fluid cell that provides ready access to the upper surface of the IRE by the AFM tip and allows for fluid exchange. The fluid cell was fitted with Omegalux cartridge heaters (CSH 10170/120V; Omega, Stamford, CT) that were controlled by a Lakeshore Cryotronics Model 331 temperature controller (Lakeshore, Westerville, OH). IR-reflective optical elements (Thorlabs, Newton, NJ) were installed in the sample compartment to facilitate alignment of the IR beam with the IRE and a KRS-5 wire-grid polarizer (Harrick Scientific Products, Pleasantville, NY) was fitted to the entrance port of the sample compartment. A schematic representation of the ATR-IR setup and the evanescent decay of the infrared beam at the IRE interface are shown in Fig. 1.

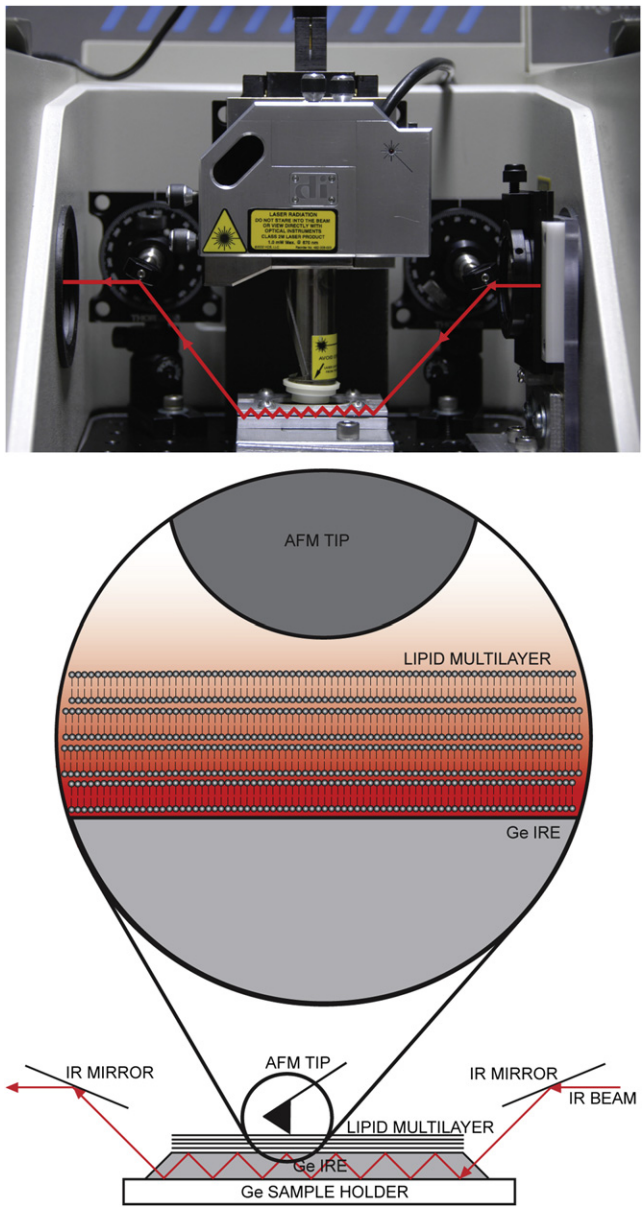


FIGURE 1 Picture (*top*) and schematic diagram (*bottom*) of an AFM scan head placed above ATR internal reflection element (IRE). The sample is placed directly in contact with the top surface of the IRE. The infrared beam is internally reflected through the length of the IRE. At each reflection, a standing electromagnetic wave of infrared light extends into the sample, and the amplitude of the wave decays exponentially with distance from the surface of the IRE.

### Atomic force microscopy (AFM)

AFM images were acquired in fluid tapping mode using 120-$\mu$m oxide-sharpened silicon nitride V-shaped DNP-S cantilever tips (Digital Instruments) installed in a combination contact/tapping mode liquid cell. All images were captured as 512 $\times$ 512 pixel images at a line scan rate of ~1 Hz. Drive frequency and amplitude set point varied depending on the tip and sample and feedback gains were optimized for each image.

AFM image analysis was conducted using the Digital Instruments Nanoscope software (version 5.30r1, Digital Instruments). Height images were subject to a first-order flatten and second-order plane-fit in the $x$-direction. Quantitative height measurements were determined by section analysis. Mean roughness was calculated using the Nanoscope software as the arithmetic average of deviations from the center plane as shown in Eq. 1,

$$R_a = \frac{\sum_i^N |Z_i - Z_{CP}|}{N}, \quad (1)$$

where $R_a$ represents the mean roughness, $Z$ represents the height in the $z$ direction, $Z_i$ is the current $Z$ position, $Z_{CP}$ is the $Z$ value of the center plane, and $N$ is the number of points within a given area.

## Attenuated total reflection infrared spectroscopy (ATR-IR)

ATR infrared spectra were collected on a Nicolet Magna 750 spectrometer equipped with a mid-range IR source, DTGS detector, and a KBr beamsplitter at a resolution of 2 $cm^{-1}$ using an average of 512 scans over a scan range of 4000–700 $cm^{-1}$ wavenumbers. All spectra were referenced against the spectra of a clean Ge IRE, and all spectra processing was carried out using the Omnic version 5.29 software (Nicolet/Thermo Electron). Infrared spectra were baseline-corrected and normalized with respect to the $CH_2$ antisymmetric stretching band at 2920 $cm^{-1}$. Determination of the secondary structure of the protein was achieved through spectral deconvolution of the amide 1 band (1700–1600 $cm^{-1}$) using the Fourier self-deconvolution (FSD) function in the Omnic software package. The FSD is carried out by first multiplying the interferogram with an exponentially increasing function, followed by an apodization function that decays to zero at a selected cutoff value. The selected cutoff value is based on the full width at half-height (FWHH) of the component bands, which are typically between 12 and 20 $cm^{-1}$ (9). The amount of resolution enhancement was defined by a factor $K$, which is the ratio of the bandwidths before and after resolution enhancement, and is typically on ~2–3 (10). All FSD spectra in this study were deconvoluted using a FWHH of 18 $cm^{-1}$ and a $K$ value of 2. Polarized spectra were collected using a wire-grid KRS-5 polarizer (Harrick Scientific Products) fitted on the entrance port to the sample chamber of the spectrometer. Spectra were collected with both $E_{||}$ (parallel to the incident plane) and $E_{\perp}$ (perpendicular to the incident plane) polarizations with FSD analyses performed for each polarization, again using FWHH and $K$ values of 18 $cm^{-1}$ and 2, respectively. Contributions of $\beta$LG in solution to the ATR spectra were subtracted before analysis.

## Germanium (Ge) internal reflection element (IRE) cleaning

To prepare the Ge IRE, it was cleaned by sonication in a basic detergent (Extran MA01; EMD Chemical, Gibbstown, NJ) and distilled water, followed by sequential immersion in methanol (Caledon Laboratories, Georgetown, Ontario, Canada) and chloroform (Sigma-Aldrich). The IRE was then dried with $N_2$ gas and subjected to 3 min plasma cleaning cycle (PDC-32G, Harrick Scientific Products).

## Sample preparation

To prepare multilamellar lipid bilayers, immediately following the cleaning procedure the lipid sample was deposited onto the surface of the IRE using a custom-built spin coater. While rotating the IRE at a rotation rate of 5000 rpm for 5 s, 30 $\mu$L of lipid dissolved in chloroform (10 mg/mL) was deposited onto the IRE surface at room temperature. The lipids, 1,2-dipalmitoyl-*sn*-glycero-3-phosphocholine (DPPC), 1,2-dimyristoyl-*sn*-glycero-3-phosphocholine (DMPC), and 1,2-dimyristoyl-*sn*-glycero-3-[phospho-*rac*-(1-glycerol)] (DMPG), were purchased from Avanti Polar Lipids (Alabaster, AL) and used without further purification. The lipid film was then hydrated with 800 $\mu$L of deuterated water ($D_2O$) or deuterated buffer (10 mM phosphate-buffed saline (PBS), 150 mM NaCl, pH 6.8), and allowed to equilibrate for 1 h before heating/or protein addition. All buffer materials and $\beta$-lactoglobulin ($\beta$LG) were purchased from Sigma-Aldrich and used without further purification. The protein, $\beta$LG, was dissolved in 10 mM PBS, 150 mM NaCl, pH 6.8 buffer at a concentration of 30 mg/mL, and added to the previously formed multilamellar lipid bilayer at a final concentration of 10 mg/mL. The sample was allowed to equilibrate with the protein for ~30 min before imaging and spectra collection. In situ AFM imaging and spectra collection, performed on the sample several hours after the initial equilibration period, were unremarkable.

## RESULTS AND DISCUSSION

### Tracking phase transitions in lipid membranes

To confirm the ability of this platform to simultaneously acquire ATR-IR spectra and in situ AFM topographical information, the thermal phase behavior of hydrated multilamellar DPPC ($T_m = 41°C$) lipid bilayers formed on the Ge IRE was examined (Fig. 2). Below the phase transition temperature, the DPPC gel phase is characterized by a high degree of acyl-chain order, whereas above the phase transition temperature in the fluid phase, the DPPC acyl chains are substantially less ordered (23–25). AFM imaging revealed that at 23°C, below the phase transition temperature of DPPC, the hydrated DPPC multilamellar lipid bilayers exhibited a root mean-square roughness, $R_a$, of ~89 nm (Fig. 2 *A*). We would note that this is the initial roughness and largely reflects the effect of the spin-coating and hydration steps on multilayer formation. Upon heating to 52°C (above $T_m = 41°C$), the multilamellar lipid bilayers appeared to flatten, undergoing a 10-fold decrease in roughness ($R_a$ = 9 nm) (Fig. 2 *B*). The straight lines in these images likely

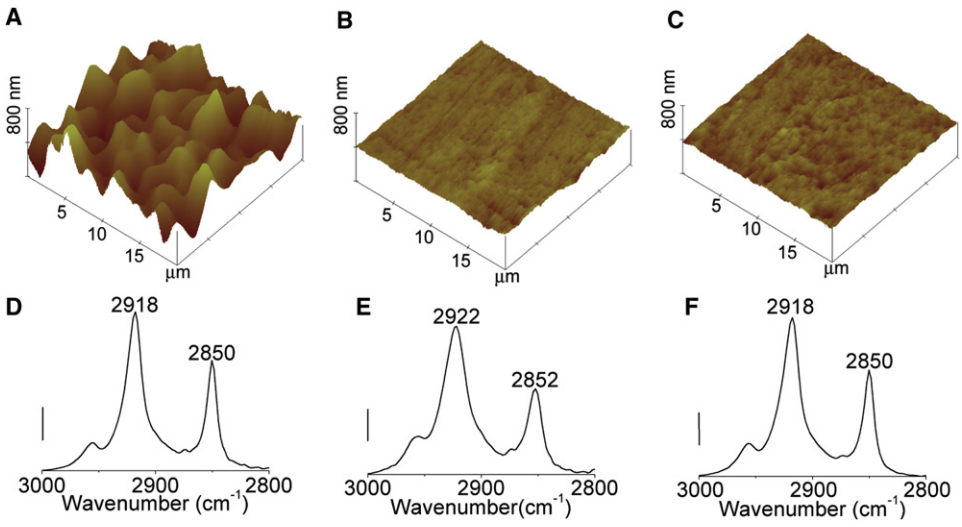


FIGURE 2 (*A–C*) AFM images of DPPC multilamellar lipid bilayers formed on a Ge IRE surface. (*A*) Partially fused DPPC multilamellar lipid bilayer at 23°C, before heating. (*B*) Fluid state DPPC multilamellar lipid bilayer at 52°C. (*C*) Gel state DPPC multilayer after cooling to 23°C. All images are shown on the same vertical scale for comparison purposes. (*D–F*) Simultaneously acquired ATR-FTIR spectra of the $CH_2$ symmetric ~2850 $cm^{-1}$, and antisymmetric ~2920 $cm^{-1}$ stretching modes are shown below their corresponding AFM images. Scale bar: 0.03 absorbance units.

reflect macroscopic scratches in the Ge IRE, illustrating the conformal nature of the now fluid-phase DPPC multilamellar lipid bilayers. During cooling through the fluid-gel transition temperature, small domains extending above the surrounding fluid phase formed, suggesting the formation of gel phase islands within the surrounding fluid phase. After heating and subsequent cooling through the phase transition, the mean roughness of the now gel-state DPPC multilamellar lipid bilayer remained approximately the same ($R_a = 8$ nm) (Fig. 2 *C*). It is important to recognize that the lipid multilayer topography that the AFM is tracking, especially after heating through the gel-fluid transition temperature and then cooling back to the gel state, reflects, to a large extent, the underlying topography of the Ge crystal. Repeated use of the crystals, including plasma cleaning to remove organic contaminants, resulted in gradual pitting of the crystal surface. Indeed, in one instance, we found that the surface roughness of a given Ge ATR crystal progressed from an as-received value of ~1.5 nm to ~11.5 nm after a single plasma cleaning cycle.

ATR-IR spectroscopy was used to track changes in the conformation of the lipid multilamellar lipid bilayers during the heating and cooling cycles. By tracking changes in the lipid spectra, changes in molecular conformation can then be correlated with topographical features resolved by AFM. For these experiments, we chose to examine the methylene ($CH_2$) stretching modes, as they are located in a region of the mid-IR spectra that is largely free of interference from bulk water bands. Changes in these bands (position, bandwidth) are diagnostic of changes in the local packing of the methylene chains. Close inspection of the methylene asymmetric and symmetric stretching modes at 2918 $cm^{-1}$ and 2850 $cm^{-1}$, respectively, revealed peak broadening and shifting that are consistent with conversion of the gel-phase DPPC lipid to a fluid phase upon heating, and reformation of the gel phase upon cooling (23–25) (Fig. 2, *D–F*).

During heating of the DPPC multilamellar lipid bilayers at 52°C, frequency shifts of 2–4 $cm^{-1}$, and peak broadening for the $CH_2$ antisymmetric and symmetric stretching modes at 2918 $cm^{-1}$ and 2850 $cm^{-1}$, were observed. The peak broadening and shifting observed for the bands indicate a more ordered gel phase below the phase transition temperature of DPPC and a more disordered liquid phase, consistent with previous data in the literature (23–27). The frequency shift from 2850 $cm^{-1}$ to 2852 $cm^{-1}$ is thought to be associated with the introduction of *gauche* conformers, which perturbs both inter- and intramolecular coupling (27). The increase in bandwidth is attributable to increased motional rates and the larger number of conformational states afforded the lipid tails in the liquid phase.

The AFM images are in good agreement with these spectral data, reflecting the morphological and topographical changes in the multilamellar lipid bilayer upon heating and cooling. It should be noted that sampling of multiple regions on the IRE surface revealed similar topographical effects.

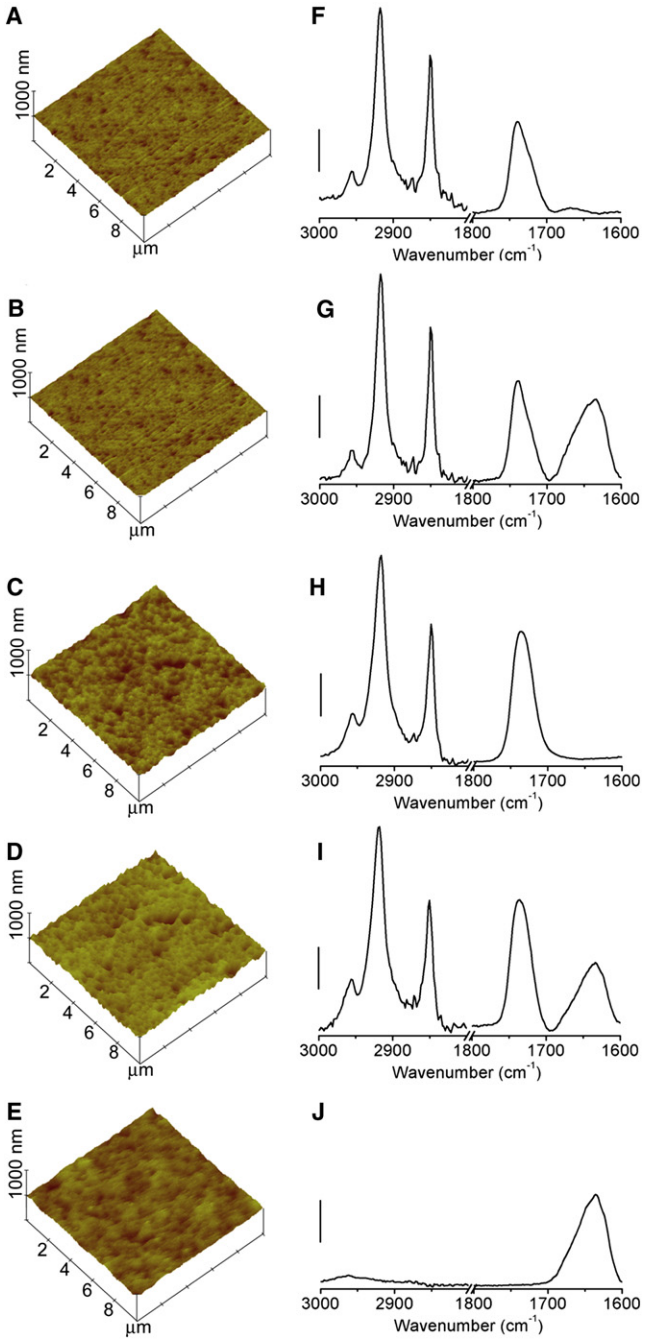


FIGURE 3 (*A–E*) AFM images of (*A*) multilamellar DMPG lipid bilayers, (*B*) multilamellar DMPG lipid bilayers, and adsorbed βLG; (*C*) multilamellar DMPC lipid bilayers, (*D*) multilamellar DMPC lipid bilayers, and adsorbed βLG; and (*E*) βLG adsorbed on to a Ge IRE surface. All images are shown on the same vertical scale for comparison purposes. (*F–J*) Simultaneously acquired ATR-FTIR spectra shown beside their corresponding AFM images. Scale bar: 0.2 absorbance units.

Since the ATR-IR technique samples a much larger area than that which can be imaged by the AFM, it is necessary to couch all the AFM images in terms of a local frame of reference. However, extensive sampling of the DPPC multilayers by in situ AFM revealed similar topographical features

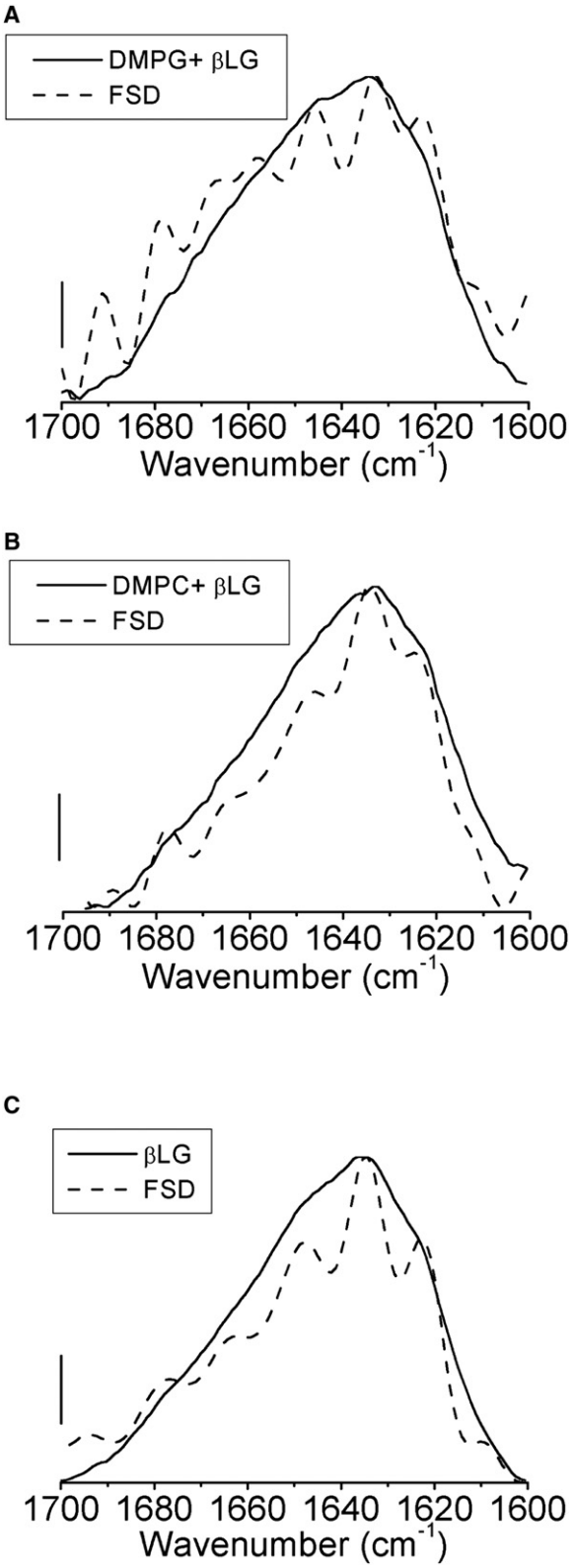


FIGURE 4 ATR-FTIR spectra for the amide 1 spectral region before and after spectral deconvolution for (*A*) DMPG multilamellar lipid bilayers after the addition of 10 mg/mL $\beta$LG in 10mM PBS 150 mM NaCl pH 6.8, (*B*) DMPC multilamellar lipid bilayers after the addition of 10 mg/mL $\beta$LG in 10mM PBS 150 mM NaCl pH 6.8, and (*C*) $\beta$LG in 10 mM PBS 150 mM NaCl pH. Deconvolution parameters: FWHH of 18 $cm^{-1}$ and K of 2. Scale bar: 0.2 absorbance units.

during heating and cooling, suggesting that these structural changes, as resolved by the AFM, were not a consequence of the scanning action of the tip.

## Tracking protein-membrane interactions

The conformation of the gl obular protein, $\beta$-lactoglobulin ($\beta$LG), is known to be strongly affected by pH (29), ionic strength (30), concentration (31), and temperature (29,30). It also known to undergo both alcohol- and lipid-induced conformational changes (32), converting from a predominantly $\beta$-sheet structure into an $\alpha$-helix conformation in the presence of anionic phospholipids (33–37). These properties prompted us to investigate whether our combined ATR-FTIR/AFM platform could resolve the interactions of $\beta$LG with model membranes, both spectroscopically and topographically, using anionic (DMPG) and zwitterionic (DMPC) lipids as our test cases.

AFM images acquired before and after the addition of $\beta$LG to supported planar multilamellar lipid bilayers of DMPG and DMPC, and a control surface comprising a clean Ge IRE, revealed little topographical contrast that could be attributed to the protein (Fig. 3). This is expected, as $\beta$LG is not known to disrupt membranes. To confirm that this lack of disruption was not due to the multilamellar nature of the lipid films on the Ge IRE, the adsorption of $\beta$LG onto unilamellar lipid bilayers of DMPG and DMPC prepared on mica was also studied by in situ AFM. These studies also confirmed that the protein did not affect the integrity of the bilayer (data not shown). The roughness of the bare Ge IRE ($R_a \cong 5$ nm) prevented facile imaging of the adsorbed protein.

ATR-FTIR spectra acquired simultaneously with AFM imaging revealed no changes in the antisymmetric and symmetric $CH_2$ stretching modes, suggesting that there was no effect of the protein on the local order in the bilayer (Fig. 3, *F–I*). To further refine our analysis of the ATR-FTIR spectra, FSD was applied on the amide 1 band for $\beta$LG in solution, and $\beta$LG adsorbed onto multilamellar lipid bilayers of DMPG and DMPC (Fig. 4). From FSD analysis, eight component bands can be resolved for the two different multilamellar lipid bilayers (Table 1). These were associated with $\beta$-sheet (1693, 1678, 1632, and 1622 $cm^{-1}$), $\alpha$-helices (1658 $cm^{-1}$), turns (1678, 1664 $cm^{-1}$), and the stretching C=C vibrations of the aromatic side chains (1610 $cm^{-1}$) (Table 1) (29,31,33–38). Close inspection of the amide 1 region and subsequent FSD deconvolution analysis revealed development of a peak at 1658 $cm^{-1}$, consistent with $\beta$LG undergoing a $\beta$-sheet to $\alpha$-helical conformational change upon binding to anionic DMPG (Fig. 4 *A*). By comparison, there is no $\alpha$-helical peak observed for the $\beta$LG protein binding to DMPC (Fig. 4 *B*). These data are in agreement with previous reports that $\beta$LG undergoes an increase in

**TABLE 1 ATR-FTIR spectral peak assignments for amide 1 band of β-lactoglobulin in deuterated 10 mM PBS 150 mM NaCl pH 6.8, and after adsorption to DMPG and DMPC multilamellar lipid bilayers**

| Peak assignment | Literature* | βLG | DMPG + βLG | DMPC + βLG |
|---|---|---|---|---|
| Aromatic C=C | 1610 | 1610 | 1611 | 1611 |
| β-sheet | 1622 | 1623 | 1623 | 1623 |
| β-sheet | 1632 | 1634 | 1632 | 1634 |
| Unordered | 1645 | 1648 | 1646 | 1646 |
| α-Helix | 1656 | — | 1658 | — |
| Turn | 1664 | 1663 | 1666 | 1664 |
| Turn\β-sheet | 1678 | 1677 | 1678 | 1678 |
| β-sheet | 1693 | 1693 | 1692 | 1690 |

*Literature values drawn from references (9,33,35,36).

α-helical content in the presence of anionic lipids, while retaining its preferred β-sheet structure in the presence of cationic lipids (33–37). FSD analysis of polarized ATR-IR spectra of the amide 1 region (~1658 $cm^{-1}$) revealed that, in the anionic DMPG bilayers, the α-helical portion of βLG was oriented largely parallel to the membrane normal, or vertical with respect to the membrane surface. The absence of α-helical character precluded any assessment of βLG orientation in the zwitterionic DMPC bilayers. The observed differences in the secondary structure of βLG in the presence of anionic (~PG), and zwitterionic (~PC) lipids clearly demonstrate that surface charge of the membrane and net protein charge are key factors in βLG-membrane interactions that cannot be deduced from AFM images alone.

## CONCLUSIONS

An integrated AFM and ATR-FTIR platform has been developed to study molecular self-assembly at model membrane interfaces. It addresses key limitations of the individual techniques by providing direct correlation between structural and topographical features resolved by AFM with spectroscopic details of molecular structure and conformation. Furthermore, although AFM is a high-resolution imaging technique that can provide detailed topographical information, it is unable to address specific details of inter- and intramolecular bonding. The instrumentation platform described here provides the ability to track changes topographically while simultaneously following protein-membrane bonding interactions and secondary structure changes through infrared spectroscopy. This integrated approach addresses a particularly critical limitation associated with AFM studies of protein-membrane interactions, namely cases in which upon binding, the protein or molecule of interest inserts into the membrane and is no longer topographically distinct from the membrane. Furthermore, this platform is well suited for visualizing structural transformations—domain movement, defect formation, aggregation—while simultaneously tracking change in vibrational spectra that would reflect changes in molecular conformation and both intra- and intermolecular interactions. Work is currently underway to study the mechanisms of antimicrobial peptide action at membranes, including peptide-induced membrane restructuring and membrane-induced protein folding using this correlated approach.

We thank the Canada Research Chairs program (to C.M.Y.), the Advanced Food and Materials Network Centre of Excellence (to J.V.), and the Canadian Institutes of Health research grant No. ITG-70196 for support of this work. We appreciate the donation of the Magna 750 FT-IR spectrometer from Eli Lilly Canada and Eli Lilly and Company. J.V. acknowledges support from a University of Toronto Graduate Open Fellowship.

## REFERENCES

1. Alattia, J. R., J. E. Shaw, C. M. Yip, and G. G. Privé. 2006. Direct visualization of saposin remodeling of lipid bilayers. *J. Mol. Biol.* 362:943–953.
2. Alattia, J. R., J. E. Shaw, C. M. Yip, and G. G. Privé. 2007. Molecular imaging of membrane interfaces reveals mode of β-glucosidase activation by saposin C. *Proc. Natl. Acad. Sci. USA.* 104:17394–17399.
3. Shaw, J. E., R. F. Epand, R. M. Epand, Z. Li, R. Bittman, et al. 2006. Correlated fluorescence-atomic force microscopy of membrane domains: structure of fluorescence probes determines lipid localization. *Biophys. J.* 90:2170–2178.
4. Shaw, J. E., R. F. Epand, J. C. Y. Hsu, G. C. H. Mo, R. M. Epand, et al. 2008. Cationic peptide-induced remodeling of model membranes: direct visualization by *in situ* atomic force microscopy. *J. Struct. Biol.* 162:121–138.
5. Shaw, J. E., R. F. Epand, K. Sinnathamby, Z. Li, R. Bittman, et al. 2006. Tracking peptide-membrane interactions: insights from in situ coupled confocal-atomic force microscopy imaging of Nap-22 peptide insertion and assembly. *J. Struct. Biol.* 155:458–469.
6. Shaw, J. E., A. Slade, and C. M. Yip. 2003. Simultaneous in situ total internal reflectance fluorescence/atomic force microscopy studies of DPPC/DOPC microdomains in supported planar lipid bilayers. *J. Am. Chem. Soc.* 125:11838–11839.
7. Slade, A. L., J. S. Schoeniger, D. Y. Sasaki, and C. M. Yip. 2006. In situ scanning probe microscopy studies of tetanus toxin-membrane interactions. *Biophys. J.* 91:4565–4574.
8. Yip, C. M., and J. McLaurin. 2001. Amyloid-β peptide assembly: a critical step in fibrillogenesis and membrane disruption. *Biophys. J.* 80:1359–1371.
9. Goormaghtigh, E., V. Raussens, and J. M. Ruysschaert. 1999. Attenuated total reflection infrared spectroscopy of proteins and lipids in biological membranes. *Biochim. Biophys. Acta.* 1422:105–185.
10. Tamm, L. K., and S. A. Tatulian. 1997. Infrared spectroscopy of proteins and peptides in lipid bilayers. *Q. Rev. Biophys.* 30:365–429.
11. Gremlich, H. U., U. P. Fringeli, and R. Schwyzer. 1983. Conformational changes of adrenocorticotropin peptides upon interaction with lipid membranes revealed by infrared attenuated total reflection spectroscopy. *Biochemistry.* 22:4257–4264.
12. Gremlich, H. U., U. P. Fringeli, and R. Schwyzer. 1984. Interaction of adrenocorticotropin-(11–24)-tetradecapeptide with neutral lipid membranes revealed by infrared attenuated total reflection spectroscopy. *Biochemistry.* 23:1808–1810.
13. Erne, D., and R. Schwyzer. 1987. Membrane structure of bombesin studied by infrared spectroscopy. Prediction of membrane interactions of gastrin-releasing peptide, neuromedin B, and neuromedin C. *Biochemistry.* 26:6316–6319.
14. Bauer, H. H., M. Muller, J. Goette, H. P. Merkle, and U. P. Fringeli. 1994. Interfacial adsorption and aggregation associated changes in secondary structure of human calcitonin monitored by ATR-FTIR spectroscopy. *Biochemistry.* 33:12276–12282.
15. Badilescu, S., and C. Sandorfy. 1988. Infrared attenuated total reflection spectroscopic studies on the hydration of the gramicidin A transmembrane channel. *J. Mol. Struct.* 189:31–42.

16. Kota, Z., T. Pali, and D. Marsh. 2004. Orientation and lipid-peptide interactions of gramicidin A in lipid membranes: polarized attenuated total reflection infrared spectroscopy and spin-label electron spin resonance. *Biophys. J.* 86:1521–1531.

17. Okamura, E., J. Umemura, and T. Takenaka. 1986. Orientation of gramicidin D incorporated into phospholipid multibilayers: a Fourier transform infrared-attenuated total reflection spectroscopic study. *Biochim. Biophys. Acta Biomembr.* 856:68–75.

18. Frey, S., and L. K. Tamm. 1991. Orientation of melittin in phospholipid bilayers. A polarized attenuated total reflection infrared study. *Biophys. J.* 60:922–930.

19. Castano, S., and B. Desbat. 2005. Structure and orientation study of fusion peptide fp23 of gp41 from HIV-1 alone or inserted into various lipid membrane models (mono-, bi- and multi-bilayers) by FT-IR spectroscopies and Brewster angle microscopy. *Biochim. Biophys. Acta Biomembr.* 1715:81–95.

20. Martin, I., H. Schaal, A. Scheid, and J. M. Ruysschaert. 1996. Lipid membrane fusion induced by the human immunodeficiency virus type 1 gp41 N-terminal extremity is determined by its orientation in the lipid bilayer. *J. Virol.* 70:298–304.

21. Arkin, I. T., M. Rothman, C. F. C. Ludlam, S. Aimoto, D. M. Engelman, et al. 1995. Structural model of the phospholamban ion channel complex in phospholipid membranes. *J. Mol. Biol.* 248:824–834.

22. Brucherseifer, M., C. Kranz, and B. Mizaikoff. 2007. Combined in situ atomic force microscopy-infrared-attenuated total reflection spectroscopy. *Anal. Chem.* 79:8803–8806.

23. Cameron, D. G., H. L. Casal, E. F. Gudgin, and H. H. Mantsch. 1980. The gel phase of dipalmitoyl phosphatidylcholine. An infrared characterization of the acyl chain packing. *Biochim. Biophys. Acta Biomembr.* 596:463–467.

24. McElhaney, R. N. 1982. The use of differential scanning calorimetry and differential thermal analysis in studies of model and biological membranes. *Chem. Phys. Lipids.* 30:229–259.

25. Okamura, E., J. Umemura, and T. Takenaka. 1990. Orientation studies of hydrated dipalmitoylphosphatidylcholine multibilayers by polarized FTIR-ATR spectroscopy. *Biochim. Biophys. Acta Biomembr.* 1025:94–98.

26. Cameron, D. G., and H. H. Mantsch. 1978. The phase transition of 1,2-dipalmitoyl-*sn*-glycero-3-phosphocholine as seen by Fourier transform infrared difference spectroscopy. *Biochem. Biophys. Res. Commun.* 83:886–892.

27. Casal, H. L., and H. H. Mantsch. 1984. Polymorphic phase behavior of phospholipid membranes studied by infrared spectroscopy. *Biochim. Biophys. Acta.* 779:381–401.

28. Reference deleted in proof.

29. Casal, H. L., U. Kohler, and H. H. Mantsch. 1988. Structural and conformational changes of $\beta$-lactoglobulin B: an infrared spectroscopic study of the effect of pH and temperature. *Biochim. Biophys. Acta.* 957:11–20.

30. Aymard, P., D. Durand, and T. Nicolai. 1996. The effect of temperature and ionic strength on the dimerization of $\beta$-lactoglobulin. *Int. J. Biol. Macromol.* 19:213–221.

31. Lefèvre, T., and M. Subirade. 1999. Structural and interaction properties of $\beta$-lactoglobulin as studied by FTIR spectroscopy. *Int. J. Food Sci. Technol.* 34:419–428.

32. Dong, A., J. Matsuura, M. C. Manning, and J. F. Carpenter. 1998. Intermolecular $\beta$-sheet results from trifluoroethanol-induced nonnative $\alpha$-helical structure in $\beta$-sheet predominant proteins: infrared and circular dichroism spectroscopic study. *Arch. Biochem. Biophys.* 355:275–281.

33. Bhattacharjee, C., S. Saha, A. Biswas, M. Kundu, L. Ghosh, et al. 2005. Structural changes of $\beta$-lactoglobulin during thermal unfolding and refolding—an FT-IR and circular dichroism study. *Protein J.* 24:27–35.

34. Lefèvre, T., and M. Subirade. 2000. Interaction of β-lactoglobulin with phospholipid bilayers: a molecular level elucidation as revealed by infrared spectroscopy. *Int. J. Biol. Macromol.* 28:59–67.

35. Lefèvre, T., and M. Subirade. 2001. Conformational rearrangement of $\beta$-lactoglobulin upon interaction with an anionic membrane. *Biochim. Biophys. Acta Protein Struct. Mol. Enzymol.* 1549:37–50.

36. Zhang, X., N. Ge, and T. A. Keiderling. 2007. Electrostatic and hydrophobic interactions governing the interaction and binding of $\beta$-lactoglobulin to membranes. *Biochemistry.* 46:5252–5260.

37. Zhang, X., and T. A. Keiderling. 2006. Lipid-induced conformational transitions of $\beta$-lactoglobulin. *Biochemistry.* 45:8444–8452.

38. Dong, A., J. Matsuura, S. D. Allison, E. Chrisman, M. C. Manning, et al. 1996. Infrared and circular dichroism spectroscopic characterization of structural differences between $\beta$-lactoglobulin A and B. *Biochemistry.* 35:1450–1457.